



# Photoacoustic Tomography in Cardiovascular Medicine: Innovations in Assessing Hemodynamics and Metabolic Function

Yilin Luo<sup>1</sup> · Lihong V. Wang<sup>1,2</sup>

Accepted: 12 May 2025

© The Author(s), under exclusive licence to Springer Science+Business Media, LLC, part of Springer Nature 2025

## Abstract

**Purpose of Review** Photoacoustic tomography (PAT) has emerged as a promising non-ionizing imaging modality that leverages optical absorption contrast to provide anatomical, functional, and metabolic insights. This review highlights recent advancements in PAT for assessing hemodynamics and metabolic function in the diagnosis, treatment, and monitoring of cardiovascular diseases (CVDs).

**Recent Findings** PAT has been applied to evaluate vascular morphology, blood flow, perfusion, and cardiac hemodynamics. It has also been used for metabolic assessments, including oxygenation, lipid accumulation, glucose dynamics, collagen distribution, and inflammatory responses.

**Summary** By selecting appropriate wavelengths, PAT can target specific molecular contrasts, while multi-wavelength imaging enables simultaneous visualization of multiple biomarkers. These capabilities provide a comprehensive view of CVD progression and treatment. Ongoing technological advancements, clinical trials, and translational efforts are essential for validating PAT's clinical utility and accelerating its integration into routine cardiovascular care.

**Keywords** Photoacoustic imaging · Cardiovascular imaging · Metabolic function · Cardiovascular hemodynamics · Atherosclerosis · Myocardial infarction

## Opinion Statement

PAT has the potential to bridge the gap between existing imaging modalities for CVD by offering a hybrid approach that uniquely combines deep penetration, rapid acquisition, high spatial-resolution and molecular specificity without ionizing radiation.

Its broad application in cardiovascular disease spans multiple areas. In myocardial infarction, PAT enables real-time mapping of myocardial oxygenation and perfusion deficits, aiding in early detection and risk assessment. For atherosclerosis, it provides both intravascular and non-invasive

solutions to characterize plaque structure and composition, helping to identify vulnerable plaques. In peripheral artery disease (PAD), PAT assesses blood flow and tissue oxygenation, improving diagnostic accuracy and treatment monitoring. Additionally, PAT has shown promise in detecting thrombosis, skin inflammation, ischemia, and diabetes-related vascular changes. By utilizing multiple wavelengths, PAT enables label-free characterization of multiple biomarkers, providing a comprehensive and synchronized analysis of the complex interplay of factors driving CVD. Integrating these physiological markers offers a holistic understanding of CVD progression and therapeutic response.

Ongoing technological advancements and research efforts support PAT's strong potential for clinical translation. As development continues, PAT is poised to become a powerful tool in cardiovascular medicine, improving disease detection, monitoring, and treatment strategies.

✉ Lihong V. Wang  
LVW@caltech.edu

<sup>1</sup> Caltech Optical Imaging Laboratory, Andrew and Peggy Cherng Department of Medical Engineering, California Institute of Technology, 1200 East California Boulevard, Pasadena, CA 91125, USA

<sup>2</sup> Caltech Optical Imaging Laboratory, Department of Electrical Engineering, California Institute of Technology, 1200 East California Boulevard, Pasadena, CA 91125, USA

## Introduction

Cardiovascular diseases (CVDs) have remained the leading cause of death in the United States for over a century, accounting for approximately 1 million deaths in 2024 [1]. The high mortality and morbidity rates associated with CVDs pose both a public health challenge and a substantial financial burden on healthcare systems worldwide [2]. Early and accurate diagnosis, effective intervention, and continuous monitoring are essential for improving patient outcomes and reducing healthcare costs. In the clinical management of CVDs, medical imaging has been an indispensable tool, providing crucial insights into cardiovascular structure, function, and metabolic activities. Clinicians often rely on various complementary imaging modalities to unravel the complexity of CVDs, each with distinct advantages and limitations (Table 1).

Computed Tomography (CT) provides high-resolution, rapid anatomical imaging of coronary arteries. With the injection of contrast dyes, Coronary CT angiography (CTA) enables non-invasive assessment of coronary artery disease (CAD) by visualizing vessel lumen narrowing and calcification [14]. However, CT expose patients to ionizing radiation and contrast agents, which may be risky for patients with renal impairment. Magnetic Resonance Imaging (MRI) offers exceptional soft tissue contrast and functional imaging without radiation, making it valuable for vessel morphology, ventricular function, myocardial infarction, and plaque characterization [15]. However, MRI is time-intensive, expensive, and unsuitable for patients with metallic implants. Positron Emission Tomography (PET) enables metabolic and molecular imaging by detecting radiotracer uptake, allowing assessment of metabolic or inflammatory processes [16]. Despite high sensitivity, PET suffers from limited spatial resolution and reliance on radioactive tracers. Ultrasound (US) imaging is widely used for cardiovascular assessment due to its accessibility, real-time capabilities, and non-ionizing radiation [17]. However, it lacks

molecule-specific contrast unless integrated with contrast agents.

Among emerging technologies, photoacoustic tomography (PAT) presents a promising hybrid approach that uniquely combines deep penetration, rapid acquisition, high spatial-resolution and molecular specificity without ionizing radiation (Table 1) [9, 18, 19]. It leverages the rich intrinsic optical absorption contrast in biological tissue – such as hemoglobin, lipids, collagen, and melanin – to provide anatomical, functional, metabolic insights into vasculature, hemodynamics and metabolism. Its cost-effectiveness and portability, coupled with comprehensive multiscale imaging capabilities, position PAT as a promising tool for advancing cardiovascular diagnostics and monitoring [7]. This review highlights recent advances in PAT for cardiovascular medicine, focusing on its applications in cardiovascular hemodynamics and metabolic function.

## Treatment Options

### Fundamentals of PAT

PAT is a hybrid imaging modality that combines the advantages of optical excitation with those of acoustic detection. In photoacoustic tomography, a short, non-ionizing laser pulse irradiates the biological tissue, where specific chromophores absorb the optical energy, leading to localized heating and subsequent thermoelastic expansion. This rapid expansion generates broadband ultrasound waves, which propagate through the tissue and are detected by ultrasound transducers. By analyzing the time-of-flight of the photoacoustic (PA) signals, the spatial distribution of the absorbers within the tissue can be accurately reconstructed. The optical excitation offers rich absorption contrast, while the acoustic detection enables deeper tissue penetration due to the reduced scattering of ultrasound waves compared to light [9].

**Table 1** Comparison of photoacoustic tomography with clinical medical imaging modalities for cardiovascular diseases

Characteristics	CT	MRI	PET	US	PAT
Spatial resolution	High (0.5–1.5 mm) [3]	High (0.5–1.5 mm) [4]	Low (2–5 mm) [5]	High* (0.1–3 mm) [6]	High* (1 $\mu$ m-1 mm) [7]
Molecular sensitivity	None**	High	High	None**	High
Functional imaging	None**	Excellent	Excellent	Excellent	Excellent
Imaging depth	Whole body	Whole body	Whole body	< 15 cm [8]	< 7 cm [9]
Temporal resolution	High (ms) [10]	Moderate (> 1s) [11]	Low (seconds) [12]	High (ms-s) [8]	High (ms-s) [13]
Ionizing radiation	Yes	No	Yes	No	No
Multiscale imaging	No	No	No	Yes	Yes
Cost and complexity	High	High	High	Low	Moderate

\*Depending on the frequency/wavelength used

\*\*Available with contrast agents

Abbreviations: *CT*, computed tomography; *MRI*, magnetic resonance imaging; *PET*, positron emission tomograph; *US*, ultrasound; *PAT*, photoacoustic tomography

By adjusting the optical excitation wavelength, PAT selectively visualizes different intrinsic biomolecules based on their unique absorption spectrum [20]. In the visible and near-infrared (NIR) region, hemoglobin's strong absorption facilitates label-free imaging of vascular networks, providing quantitative insights into angiogenesis [21], blood oxygenation dynamics [22], and vascular morphology [23]. Similarly, collagen and lipids exhibit distinct NIR absorption signatures, making PAT particularly valuable for monitoring lipid-rich plaques in arterial-related diseases [24, 25]. Beyond endogenous contrast, PAT's molecular imaging capabilities can be further augmented with exogenous agents, including metallic nanoparticles [26], small-molecule dyes [27], and genetically-encoded chromophores [28], which enhance both signal-to-noise ratio and specificity for targeted biological processes.

PAT is inherently a multi-scale approach, offering resolution that scales with imaging depth [9]. This unique capability addresses diverse cardiovascular imaging needs, spanning from cellular-level microvasculature formation to organ-level perfusion assessment. PAT has been implemented in three main configurations: photoacoustic microscopy (PAM), photoacoustic tomography (PACT), and photoacoustic endoscopy (PAE). While PAM and PAE excel at micrometer resolution within millimeter depths, PACT demonstrates versatility across both microscopic and macroscopic regimes, achieving penetration depths up to several centimeters while maintaining millimeter resolution.

### Hemodynamics Assessment

Blood is a primary biological absorber in both visible and NIR wavelength ranges in PAT. This intrinsic contrast enables the assessment of critical hemodynamics that are important for understanding and evaluating cardiovascular disorders without exogenous label.

### Vascular Morphology

Vascular morphology imaging provides essential structural context by assessing vessel dimensions, wall integrity, branching patterns, and geometric features that influence hemodynamic behavior. PAT's multiscale imaging capabilities enable comprehensive vascular imaging across multiple scales and applications.

In animal models, microvasculature is frequently studied using PAM [29, 30], which has achieved high-resolution imaging of extensive microvascular networks. Notable examples include imaging the developing cardio-cerebrovascular network in embryonic zebrafish at 1.3  $\mu\text{m}$  spatial resolution [31], and visualizing entire cerebral vascular networks in mice at single capillary level across a field of view

exceeding  $6 \times 8 \text{ mm}^2$  [32]. PAM has enabled longitudinal monitoring of wound angiogenesis in mouse skin, revealing impaired vascular network remodeling during wound healing [21]. Additionally, *in vivo* observations of hyperglycemia-induced arteriolar vasoconstriction in rat extremities have provided insights into the relationship between diabetes and CVDs [33]. Human microvasculature has also been studied non-invasively using PAT. For instance, PAT has enabled single-cell characterization of the human cuticle, providing not only morphological details but also functional insights such as flow speed and oxygen pressure [34]. In a clinical study involving 26 subjects, PAT identified disease-related morphological features in the skin microvasculature, suggesting potential PACT-derived biomarkers associated with CVD and carotid artery disease [35]. Moreover, PACT has been utilized to assess macrovascular endothelial function by measuring arterial wall distensibility through changes in vessel dimensions and diameter. This capability highlights PACT's potential as an alternative to ultrasonography for clinical flow-mediated dilation measurements [36], a key indicator of CVD risk.

PACT has been well-demonstrated in human macrovascular vessels *in vivo*. A single-breath-hold photoacoustic computed tomography revealed detailed angiographic structures in human breasts up to 4 cm deep with 255  $\mu\text{m}$  resolution [37, 38]. The detected vascular density and irregularities in vessel morphology effectively assessed responses to neoadjuvant chemotherapy, as confirmed by histopathological diagnosis [37]. In the human brain, PACT imaging of scalp vessels revealed more veins than MRI, demonstrating its potential for diagnosing cerebrovascular diseases [39]. Furthermore, a handheld PACT system successfully visualized the entire carotid bifurcation, aiding in carotid disease assessment [40]. A similar system also imaged macrovascular structures in the extremities, including the posterior tibial and dorsalis pedis arteries, highlighting its potential for peripheral artery disease (PAD) diagnostics [41].

### Blood Flow and Perfusion

Blood flow profile, including velocity and direction, are critical hemodynamic parameters in CVDs to characterize the functionality of the circulatory system. PAT enables non-invasive blood flow imaging through various mechanisms [42], such as doppler shift [43], density tracking [44], transit time [45], and amplitude encoding [46]. For a long time, *in vivo* blood flow imaging had been limited to shallow depths ( $<1 \text{ mm}$ ) due to optical scattering, with demonstration primarily in small animals, including the mouse ear [47], mouse brain [48] or zebrafish heart [49]. The first application of PAT for human blood flow measurement was demonstrated in the radial artery and veins, though it required

cuffing to enhance flow contrast in deeper tissues [50]. Recently, photoacoustic vector tomography (PAVT) has extended the imaging depths beyond 5 mm by leveraging the heterogeneity of blood flow [51]. PAVT was validated in vivo, generating flow vector maps within the vasculature of the hand and arm at depths exceeding 5 mm (Fig. 1a). This technique has revealed deviations from typical laminar flow at irregular interfaces, such as valve regions, and has enabled functional assessments of deep vessels, including flow velocity changes induced by blood pressure cuff inflation and release. Beyond blood flow assessment, PAI shows promise for detecting other dynamic contrast agents, such as circulating clots, for thrombosis diagnosis [52, 53].

Recent advances in high-framerate PACT have significantly enhanced blood perfusion monitoring capabilities in human. Multispectral PACT enables label-free imaging of forearm muscle perfusion and oxygenation under arterial and venous occlusion, advancing assessment of acute limb ischemia and venous thrombosis [35]. A follow-up clinical study from the same team revealed distinct dynamics of hemoglobin parameters in skeletal muscle during cuff-induced ischemia, with significantly impaired oxygenated hemoglobin, total hemoglobin, and oxygen saturation (SO<sub>2</sub>) levels in PAD patients compared to healthy volunteers [54]. For diabetes mellitus patients, PACT demonstrated unique peripheral hemodynamic responses and lower SO<sub>2</sub> levels during vascular occlusion, indicating its potential for monitoring vascular dysfunction [55]. PACT has also been shown to accurately identify patients with severe anemia triggering red blood cell (RBC) transfusion based on a strong positive correlation of PACT signal intensity and hemoglobin concentration [56]. Recent technological innovations include ultrafast volumetric imaging at 1 kHz, enabling longitudinal monitoring of hemodynamics in superficial vessels during vascular occlusion with only a single-element transducer [57]. Additionally, a high-framerate (33 Hz) PACT system has been developed, achieving high resolution (60–120 μm) over a large field-of-view (22 × 22 × 15 mm<sup>3</sup>). This system has been demonstrated to visualize post-occlusive reperfusion and quantify microvascular changes in PAD (Fig. 1b), skin inflammation and rheumatoid arthritis [13].

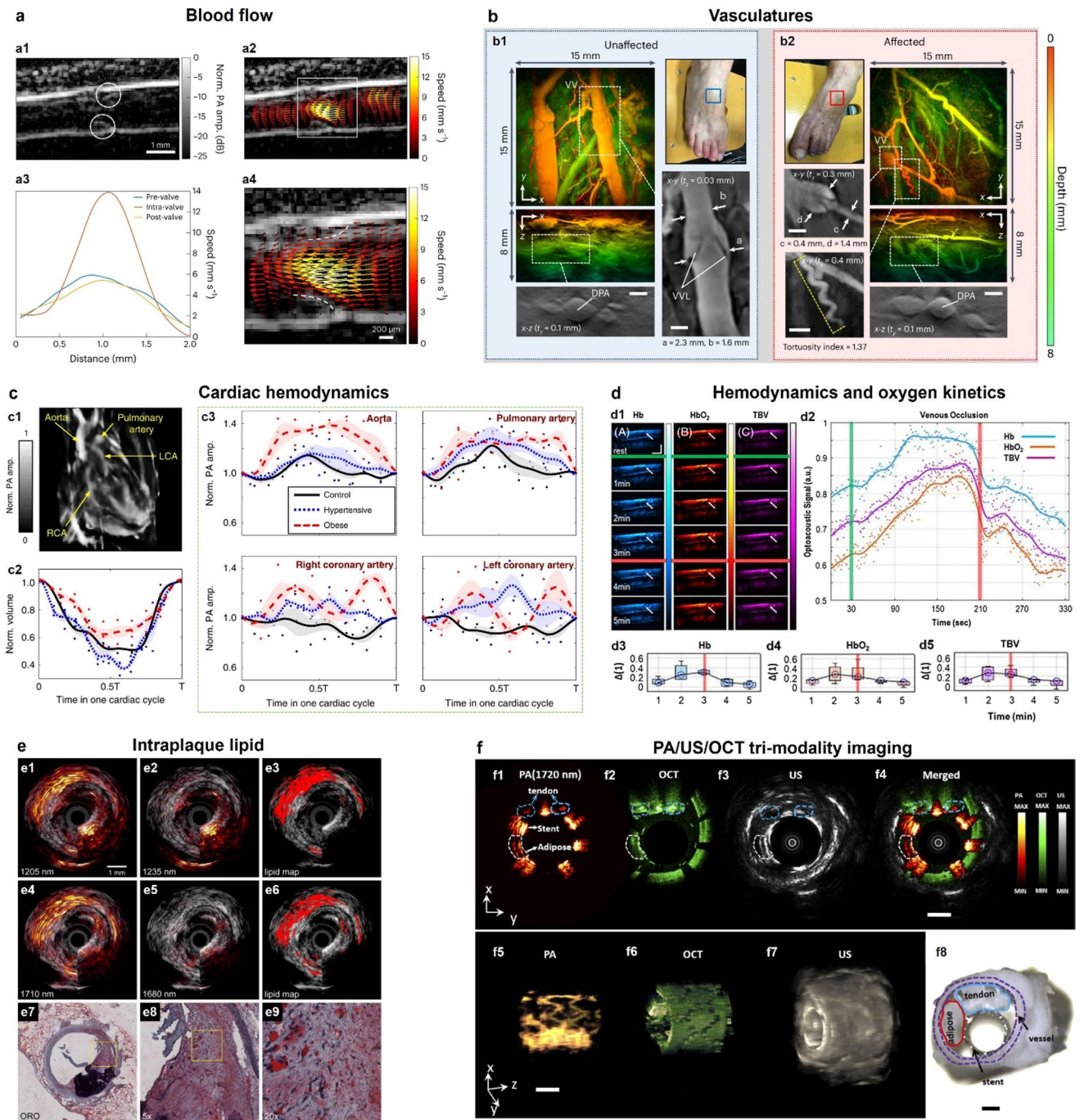
### Cardiac Hemodynamics

Cardiac hemodynamics imaging is crucial for assessing heart structure, function, and its response to CVDs. PACT is particularly well-suited for cardiac imaging in CVD research as it leverages intrinsic hemoglobin and myoglobin contrast, while providing high spatial and temporal resolution with deep tissue penetration.

For instance, a spherical-array PACT system enables four-dimensional (4D) imaging of the heart surface at

**Fig. 1** Representative cardiovascular PAT imaging results. **a**, Deep tissue blood flow PAVT imaging [51]. **a1**, A venous valve in the carpal tunnel region in the arm (valve boundaries indicated by *white circles*). **a2**, Vector overlay shows a higher speed inside the valve region than the regions upstream and downstream of the valve. **a3**, Speed profiles taken upstream, within and downstream of the valve (pre-valve, intra-valve and post-valve, respectively). **a4**, Magnified views of the maps in **a3**, with the valve boundaries indicated by the *dashed white lines*. (Panels **a1**–**a4** used with permission from: Zhang Y, et al. *Nat Biomed Eng.* 2024;8:701–11) [51]. **b**, Microvasculopathy in PAD patient feet [13]. **b1**, Unaffected right foot. **b2**, Affected left foot. DPA, dorsalis pedis artery; VV, venous valve. **c**, Cardiac hemodynamics in healthy, hypertensive, and obese hearts [62]. **c1**, A heart image shows the aorta, pulmonary artery, right coronary artery (RCA), and left coronary artery (LCA). **c2**, PA signal fluctuations in the four cardiac vasculatures among the control, hypertensive, and obese hearts ( $n=3$  for each group). **c3**, Relative changes in ventricular volume of the control (*black solid line*), hypertensive (*blue dashed line*), and hypertrophic (*red dashed line*) hearts during a cardiac cycle ( $n=3$  for each group) **d**, Forearm muscle hemodynamics and oxygen kinetics during venous occlusion [75]. **d1**, Hb, HbO<sub>2</sub>, and total blood volume (TBV) distribution within the segmented muscle area at different time points of the venous occlusion challenge. The *white arrows* point to the muscle region where the changes are more prominent. Scale bars: 1 cm. **d2**, Representative time plot (smoothing splines) of the mean optoacoustic signal for Hb, HbO<sub>2</sub> and TBV within the segmented muscle area over the whole venous occlusion challenge. Box plots of the mean change of **d3**, Hb, **d4**, HbO<sub>2</sub> and **d5**, TBV PA signal within the muscle for each minute of the venous occlusion challenge, with regard to the corresponding baseline value for all ( $n=4$ ) subjects. The *green thin stripe* corresponds to the time point of cuff inflation. The *red stripe* corresponds to the time point of the cuff deflation. **e**, Lipid detection in an atherosclerotic human coronary artery [82]. **e1**, 1205 nm and **e2**, 1235 nm combined intravascular PA/US images. **e3**, Lipid map based on 2-wavelength relative difference between the PA signal at 1205 nm and 1235 nm. **e4**, 1710 nm and **e5**, 1680 nm combined IVP/IVUS images. **e6**, Lipid map resulting from the 2-wavelength relative difference between the PA signal at 1710 nm and 1680 nm. Both lipid maps are shown overlaid on the corresponding intravascular ultrasound image. **e7**, Lipid histology stain (ORO); lipids are stained red; calcification is stained *black*. **e8**, 5× magnification of the part of the atherosclerotic plaque indicated as lipid rich by the lipid stains (area outlined in *yellow* in **e7**), shows larger extracellular lipid droplets, while the lipids in all other parts of the lesion are intracellular or contained in small extracellular droplets. **e9**, 4× magnification of area outlined in *yellow* in **e8**. **f**, Cross-sectional and 3D PAT/OCT/US images of the phantom [91]. **f1**–**f3**, PA (1720 nm), OCT, and US B-scan image, respectively. **f4**, Merged tri-modality image. **f5**–**f7**, PA, OCT, and US 3D image. **f8**, Phantom photograph. Scale bar: 1 mm

a 50 Hz frame rate with a 200 μm resolution, using multiple wavelengths to distinguish blood oxygenation states in cardiac chambers [58]. An improved system from the same team, with higher resolution (100 μm) and a faster frame rate (100 Hz), demonstrated ultrafast 4D imaging of cardiac mechanical wave propagation in an Langendorff-isolated murine heart. This approach allowed for the extraction of accurate dispersion and phase velocity maps of cardiac waves and revealed vortex-like patterns linked to mechanical phase singularities during arrhythmic events induced by ventricular stimulation [59]. The same system was further applied for noninvasive time-lapse 4D imaging



of embryonic heart development across various gestational stages (GDs 14.5–17.5) within the uterus [60]. Findings revealed a progressive increase in embryonic heart rate with development, along with synchronized ventricular contraction and relaxation, distinct from the sequential motion observed in adult hearts. Multi-wavelength imaging further captured dynamic fluctuations in blood oxygen saturation throughout the cardiac cycle, offering deeper insight into embryonic cardiovascular physiology.

PACT has also been applied for in vivo imaging of small animal hearts. A single-impulse panoramic PACT system with a ring transducer was developed, achieving 125  $\mu\text{m}$  in-plane resolution at a 50 Hz frame rate. This system provides deep tissue penetration, reaching up to 48 mm in cross-sectional width in vivo, and enables full-view imaging of the entire mouse body with anatomical, dynamical, and functional contrasts [61]. Further advancements from the team led to the development of a four-arc-shaped PACT system with isotropic 3D resolution, allowing noninvasive imaging

of rat hearts at 390  $\mu\text{m}$  resolution with an imaging depth exceeding 2 cm [62]. Optimized illumination and detection schemes minimized optical attenuation and acoustic distortion through the chest wall, enabling high-fidelity visualization of cardiac anatomy and intracardiac hemodynamics (Fig. 1c). Rapid 10-second scanning of the rat heart captured variations in cardiac chamber size, wall thickness, and hemodynamics across healthy, hypertensive, and obese rats. This breakthrough significantly enhances the capability of PACT for studying cardiac function and disease progression *in vivo*.

PACT's cardiac hemodynamic imaging has enabled multiple studies on non-invasive myocardial infarction (MI) boundary delineation, addressing a longstanding challenge unmet by other techniques. In a mouse ischemia model with left anterior descending artery ligation, the infarcted region showed an approximately 2.5-fold reduction in PA signal intensity, reflecting reduced hemoglobin concentration. Longitudinal monitoring further showed a linear correlation ( $r=0.955$ ,  $p<0.001$ ) with infarct size quantified by tripheyltetrazolium chloride staining [63]. A dual-wavelength approach targeting collagen and water absorption peaks further improved infarct size quantification by distinguishing ischemic from infarcted regions, addressing limitations of hemoglobin-only measurements. Additionally, a quantitative parameter was proposed for automated and accurate millimeter-level MI demarcation [64]. Exogenous contrast agents, including nanoparticles [65–67], organic dyes [68, 69], and interactive polymers [70], have further enhanced infarct visualization for noninvasive PAT detection.

While translating PACT cardiac imaging to humans remains challenging, technological advancements show promise. Theoretical analysis of PAT for non-invasive oxygenation imaging predicts a maximum 3 cm imaging depth – approximately the average skin-to-heart distance in human [71] – for a 50% change in PA signal using a single-element ultrasonic transducer [72]. However, recent developments in PACT have introduced a densely packed hemispheric transducer array with over 3,000 elements, significantly enhancing the signal-to-noise ratio. For MI applications, the PA signal intensity change is even greater in infarcted regions [63], potentially further extending the detection depth limit.

### Metabolic Function Assessment Using PAT

By using different wavelengths, PAT enables the localization of metabolic-related chromophores, such as oxyhemoglobin (HbO<sub>2</sub>) and deoxyhemoglobin (HbR), lipids, glucose, within tissues, providing critical information on metabolic processes associated with CVDs.

### Oxygen Metabolism

Non-invasive quantitative measurement of the blood oxygen metabolism is of the most critical functional applications of PAT. Because HbO<sub>2</sub> and HbR exhibit distinct absorption spectrum, PAT can estimate their concentrations using dual-wavelength illumination, enabling the calculation of key oxygen metabolic parameters [73].

In a study of four hemispherectomy patients, PACT detected relative blood oxygen saturation changes as small as 1% during motor tasks in the brain cortex [39], with the identified functional regions validated by blood-oxygen-level-dependent functional MRI (BOLD fMRI). Notably, PACT signals exhibited a faster onset time to peak compared to BOLD fMRI, highlighting its potential for faster detection of functional brain activation. In another study, a hybrid PACT-US system effectively distinguished the oxygenation status of the carotid artery, sternocleidomastoid muscles, thyroid lobe and jugular vein in humans [74]. The same research team used a similar system to visualize hemodynamic and oxygenation changes in skeletal muscle under arterial and venous occlusions (Fig. 1d) [75]. Arterial occlusion led to increased hemoglobin levels with stable HbO<sub>2</sub> and total blood volume (TBV), followed by a rise during the hyperemic phase. Venous occlusion, in contrast, resulted in marked increases in intramuscular HbO<sub>2</sub>, Hb, and TBV. These findings marked the first tomographic visualization of intramuscular hemodynamics under disrupted blood flow.

The ability of PACT to assess oxygenation states makes it a valuable tool for CVD diagnosis. In a pilot study of 12 patients, PACT effectively differentiated arteriovenous from venous malformations by quantifying the ratio of HbO<sub>2</sub> to HbR, offering a non-invasive biomarker for vascular anomalies [76]. Similarly, in a clinical study of 197 patients with PAD, PACT-derived HbO<sub>2</sub> reliably classified disease stages, distinguishing healthy individuals, those with intermittent claudication, and patients with critical limb-threatening ischemia (CLTI). Internal validation in 96 patients demonstrated PACT's high sensitivity (96.4%) and specificity (42.9%), with superior diagnostic accuracy in CLTI cases where conventional methods, such as the ankle-brachial index (ABI), were inconclusive [77].

### Lipid Metabolism

Lipid accumulation in the vascular wall is a critical event in atherogenesis, triggering inflammatory responses that drive fibrous plaque formation. As plaque lipids continue to accumulate, they can lead to the formation of unstable atherosclerotic plaques, which are susceptible to rupture and subsequent blood clot formation. This process significantly elevates the risk of acute coronary events, including

ischemic heart disease and stroke [78]. Currently, no clinically available imaging modality can comprehensively characterize atherosclerotic lesions to accurately assess plaque vulnerability prognostically [79]. With its intrinsic lipid contrast in the NIR region, PAT holds significant potential to bridge this gap by providing detailed imaging of both plaque structure and composition, key determinants of plaque stability, without requiring exogenous labels.

Intravascular photoacoustic imaging (IVPA) is the most intensely studied application of PAT in cardiology [80]. IVPA employs a PAE implementation, utilizing a specialized imaging catheter to deliver light and detect PA signals within arteries. The first *ex vivo* IVPA imaging of human specimens used a 1.25 mm diameter intravascular catheter to identify lipid content differences between mild fibrous intimal thickening and advanced atherosclerotic lesions [81]. A follow-up study demonstrated the potential of multi-wavelength IVPA to distinguish between plaque lipids and peri-adventitial lipids in *ex vivo* human coronary arteries (Fig. 1e), leveraging the distinct absorption signatures of various lipid compounds [82]. Real-time IVPA systems are also developed to minimize motion artifacts caused by cardiac pulsation. A portable IVPA-US system with a 16 Hz frame rate has been designed for *ex vivo* imaging of an atherosclerotic human coronary artery, showing a strong correlation with gold-standard histopathology [83].

*In vivo* IVPA studies have thus far been limited to animal models. The first *in vivo* IVPA imaging study was performed in a rabbit aorta, demonstrating the ability of IVPA to detect diffuse, lipid-rich plaques in the Watanabe heritable hyperlipidemic (WHHL) rabbit model of atherosclerosis [84]. IVPA was subsequently refined for the quantitative characterization of immature, proliferative atherosclerotic plaques [85]. In this study, pixel-based lipid relative concentration (LRC) was evaluated in the vessel walls of rabbits fed a high-fat, high-cholesterol diet. Three-dimensional LRC maps provided detailed visualization of lipid distribution, including concentration and depth within atherosclerotic plaques, with strong correlation to histological findings. Longitudinal lipid accumulation was assessed using maximum LRC, mean LRC, and high lipid content area, all of which correlated with the duration of the high-fat diet. In a large animal model, IVPA was applied for *in vivo* coronary lipid imaging in an atherosclerotic swine model using a 1 mm diameter catheter [86]. In one artery, IVPA detected extensive plaque with a strong intimal lipid signal. Another artery exhibited mild intimal thickening with sparse or no lipid content. These findings were validated through independent catheter-based imaging with intravascular optical coherence tomography (OCT) and confirmed by histological analysis.

Non-invasive lipid characterization in human carotid atherosclerosis can be achieved using multispectral PACT [87]. In a study of five patients and five healthy volunteers, a handheld multispectral PACT system visualized lipid and hemoglobin distribution through spectral unmixing. The fat-blood ratio effectively distinguished patients from healthy volunteers ( $p=0.001$ ) and differentiated plaque from lumen ( $p=0.04$ ). These results highlight PACT's potential as a molecular imaging tool for assessing carotid plaques in research and clinical settings.

### Other Metabolic Processes

Multiple other metabolic processes involved in cardiovascular diseases can be assessed with PAT. Inflammation, particularly intraplaque hemorrhage, is another critical factor in plaque vulnerability. Initial studies demonstrated the feasibility of PACT for imaging intraplaque hemorrhages in carotid plaques from human endarterectomy samples *ex vivo*, revealing the presence of intraplaque hemorrhage that were not visible in US images, validated by histological data [88]. A subsequent pilot clinical study involving 16 patients further validated PACT's ability to differentiate hemorrhagic plaques from the carotid blood pool based on distinct PA signal characteristics [89]. Additionally, PAI has shown promise in evaluating collagen remodeling, a key process in atherosclerosis progression. While excessive collagen accumulation contributes to arterial stenosis, its degradation weakens plaques, increasing rupture risk [90]. Multispectral imaging can differentiate plaque collagen and lipid based on their distinct absorption peaks, as demonstrated in *ex vivo* studies using collagen-rich phantoms (Fig. 1f) [91]. Furthermore, PACT has been explored for non-invasive glucose measurements in human epidermis using mid-infrared light [92]. This technique enables quantitative assessment of skin glucose concentrations within the clinically relevant range of less than 50 mg/dL to over 300 mg/dL. Preliminary studies in both healthy individuals and diabetes patients support its potential as a noninvasive glucose monitoring tool, essential for managing PAD risk.

### Conclusions

In this review, we have highlighted recent advancements in PAT for cardiovascular medicine, emphasizing its role in hemodynamic and metabolic assessments. PAT's unique advantages, including non-invasive molecular specificity, high spatial and temporal resolution, and deep tissue penetration, have demonstrated significant potential in various cardiovascular applications, such as blood flow and perfusion monitoring, myocardial infarction assessment,

and atherosclerosis progression evaluation. Notably, PAT's multi-wavelength capability enables the simultaneous visualization of multiple hemodynamic and metabolic contrasts, such as blood perfusion and oxygenation within the vasculature. This allows for a comprehensive and synchronized analysis of the intricate interplay of factors driving CADs, capturing dynamic interactions between ischemia, perfusion deficits, vascular remodeling, and metabolic alterations. By integrating these complex physiological markers, PAT has the potential to provide a more holistic understanding of CAD progression and therapeutic response.

Future developments in PAT include hybrid imaging systems that integrate PAT with other modalities, such as OCT [91], Raman imaging [93], ultrasound imaging [93, 94], and MRI [95], enhancing diagnostic precision through complementary imaging capabilities. Additionally, recent advances in soft electronics have opened new opportunities for PAT in wearable and flexible devices. Flexible PAT patches have been developed for continuous, non-invasive monitoring of multiple cardiovascular biomarkers, including hypoxia, intravascular exogenous agent concentration decay, and hemodynamics [96]. Another study demonstrated a wearable PAT patch capable of 3D mapping of hemoglobin in deep tissues up to 2 cm, while simultaneously assessing core temperature [97]. These innovations offer new pathways for personalized and continuous CAD management, leveraging the unique advantages of PAT.

Despite these promising developments, most studies have been conducted in human samples or small animal models and remain at the early stages of biomedical research [98]. However, PAT reached a milestone in 2021 when the Seno Imagio Breast Imaging System, which combines PAT with ultrasound, received FDA approval for breast cancer diagnosis [99]. More recently, PAT was incorporated into the Digital Imaging and Communications in Medicine (DICOM) standard in 2023, marking an important step toward its integration into routine clinical practice [18]. With ongoing technological refinements and clinical translation efforts, PAT is set to establish itself as a transformative imaging modality in cardiovascular medicine.

## Key References

- Lin L, Tong X, Cavallero S, Zhang Y, Na S, Cao R, et al. Non-invasive photoacoustic computed tomography of rat heart anatomy and function. *Light Sci Appl*. 2023;12:12.
  - This study demonstrates PAT's ability to image rat heart hemodynamics and structural changes,

providing quantitative comparisons between healthy and obese rat hearts.

- Zhang Y, Olick-Gibson J, Khadria A, Wang LV. Photoacoustic vector tomography for deep haemodynamic imaging. *Nat Biomed Eng*. 2024;8:701–11.
  - This study introduces PAT's capability for *in vivo* deep tissue flow quantification, marking a significant advancement in hemodynamic imaging.
- Park J, Choi S, Knieling F, Clingman B, Bohndiek S, Wang LV, et al. Clinical translation of photoacoustic imaging. *Nat Rev Bioeng*. 2024;1–20.
  - This review outlines the current status, challenges, and future directions for the clinical translation of PAT.

**Author Contributions** Y. L. wrote the main manuscript with guidance from L. V. W.

**Funding** This work was sponsored by the United States National Institutes of Health (NIH) grants U01 EB029823 (BRAIN Initiative), R35 CA220436 (Outstanding Investigator Award), R01 EB028277, and R01 CA282505.

**Data Availability** No datasets were generated or analysed during the current study.

## Declarations

**Human and Animal Rights and Informed Consent** This article does not contain any studies with human or animal subjects performed by any of the authors.

**Conflict of interest** L.V.W. has a financial interest in Microphotoacoustics, Inc., CalPACT, LLC, and Union Photoacoustic Technologies, Ltd., which did not support this work. L.V.W. also reports numerous patents.

## References

1. Martin SS, Aday AW, Almarzooq ZI, Anderson CAM, Arora P, Avery CL, et al. 2024 heart disease and stroke statistics: a report of US and global data from the American heart association. *Circulation*. 2024;149:e347–913.
2. Tarride J-E, Lim M, DesMeules M, Luo W, Burke N, O'Reilly D, et al. A review of the cost of cardiovascular disease. *Can J Cardiol*. 2009;25:e195–202.
3. Flohr TG, Raupach R, Bruder H. Cardiac CT: how much can temporal resolution, spatial resolution, and volume coverage be improved? *J Cardiovasc Comput Tomogr*. 2009;3:143–52.
4. Kramer CM, Barkhausen J, Bucciarelli-Ducci C, Flamm SD, Kim RJ, Nagel E. Standardized cardiovascular magnetic resonance imaging (CMR) protocols: 2020 update. *J Cardiovasc Magn Reson*. 2020;22:17.

5. Lassen ML, Kwiecinski J, Slomka PJ. Gating approaches in cardiac PET imaging. *PET Clin.* 2019;14:271–9.
6. Perez-Liva M, Yoganathan T, Herraiz JL, Porée J, Tanter M, Balvay D, et al. Ultrafast ultrasound imaging for super-resolution preclinical cardiac PET. *Mol Imaging Biol.* 2020;22:1342–52.
7. Karlas A, Fasoula N-A, Paul-Yuan K, Reber J, Kallmayer M, Bozhko D, et al. Cardiovascular optoacoustics: from mice to men – a review. *Photoacoustics.* 2019;14:19–30.
8. Cikes M, Tong L, Sutherland GR, D'hooge J. Ultrafast cardiac ultrasound imaging: technical principles, applications, and clinical benefits. *JACC: Cardiovasc Imaging.* 2014;7:812–23.
9. Wang LV, Hu S. Photoacoustic tomography: in vivo imaging from organelles to organs. *Science.* 2012;335:1458–62.
10. Ramjattan NA, Lala V, Kousa O, Shams P, Makaryus AN. Coronary CT Angiography. *StatPearls* [Internet]. Treasure Island (FL): StatPearls Publishing; 2025 [cited 2025 Feb 16]. Available from: <http://www.ncbi.nlm.nih.gov/books/NBK470279/>
11. Tseng W-YI, Su M-YM, Tseng Y-HE. Introduction to cardiovascular magnetic resonance: technical principles and clinical applications. *Acta Cardiol Sin.* 2016;32:129–44.
12. Nekolla SG, Rischpler C, Higuchi T. Preclinical imaging of cardiovascular disease. *Semin Nucl Med.* 2023;53:586–98.
13. Huynh NT, Zhang E, Francies O, Kuklis F, Allen T, Zhu J et al. A fast all-optical 3D photoacoustic scanner for clinical vascular imaging. *Nat Biomed Eng.* 2024;1–18.
14. Budoff MJ, Achenbach S, Blumenthal RS, Carr JJ, Goldin JG, Greenland P, et al. Assessment of coronary artery disease by cardiac computed tomography. *Circulation.* 2006;114:1761–91.
15. Constantine G, Shan K, Flamm SD, Sivanathan MU. Role of MRI in clinical cardiology. *Lancet.* 2004;363:2162–71.
16. Gaemperli O, Kaufmann PA. PET and PET/CT in cardiovascular disease. *Ann N Y Acad Sci.* 2011;1228:109–36.
17. Dave JK, Mc Donald ME, Mehrotra P, Kohut AR, Eisenbrey JR, Forsberg F. Recent technological advancements in cardiac ultrasound imaging. *Ultrasonics.* 2018;84:329–40.
18. Park J, Choi S, Knieling F, Clingman B, Bohndiek S, Wang LV et al. Clinical translation of photoacoustic imaging. *Nat Rev Biomed Eng.* 2024;1–20.
19. Knieling F, Lee S, Ntziachristos V. A primer on current status and future opportunities of clinical optoacoustic imaging. *Npj Imaging.* 2025;3:1–16.
20. Weber J, Beard PC, Bohndiek SE. Contrast agents for molecular photoacoustic imaging. *Nat Methods.* 2016;13:639–50.
21. Rebling J, Ben-Yehuda Greenwald M, Wietecha M, Werner S, Razansky D. Long-term imaging of wound angiogenesis with large scale optoacoustic microscopy. *Adv Sci.* 2021;8:2004226.
22. Tzoumas S, Nunes A, Olefir I, Stangl S, Symvoulidis P, Glasl S, et al. Eigenspectra optoacoustic tomography achieves quantitative blood oxygenation imaging deep in tissues. *Nat Commun.* 2016;7:12121.
23. Yang Z, Chen J, Yao J, Lin R, Meng J, Liu C, et al. Multi-parametric quantitative microvascular imaging with optical-resolution photoacoustic microscopy in vivo. *Opt Express.* 2014;22:1500–11.
24. He Y, Shi J, Pleitez MA, Maslov K, Wagenaar DA, Wang LV. Label-free imaging of lipid-rich biological tissues by mid-infrared photoacoustic microscopy. *J Biomed Opt.* 2020;25:106506.
25. Jansen K, van der Steen AFW, Wu M, van Beusekom HMM, Springeling G, Li X, et al. Spectroscopic intravascular photoacoustic imaging of lipids in atherosclerosis. *J Biomed Opt.* 2014;19:026006.
26. Taruttis A, Herzog E, Razansky D, Ntziachristos V. Real-time imaging of cardiovascular dynamics and circulating gold nanorods with multispectral optoacoustic tomography. *Opt Express OE.* 2010;18:19592–602.
27. Vinegoni C, Botnaru I, Aikawa E, Calfon MA, Iwamoto Y, Folco EJ, et al. Indocyanine green enables near-infrared fluorescence imaging of lipid-rich, inflamed atherosclerotic plaques. *Sci Transl Med.* 2011;3:84ra45.
28. Razansky D, Distel M, Vinegoni C, Ma R, Perrimon N, Köster RW, et al. Multispectral opto-acoustic tomography of deep-seated fluorescent proteins in vivo. *Nat Photon.* 2009;3:412–7.
29. Yeh C, Soetikno B, Hu S, Maslov KI, Wang LV. Microvascular quantification based on contour-scanning photoacoustic microscopy. *J Biomed Opt.* 2014;19:096011.
30. Yang Z, Chen J, Yao J, Lin R, Meng J, Liu C, et al. Multi-parametric quantitative microvascular imaging with optical-resolution photoacoustic microscopy in vivo. *Opt Express OE.* 2014;22:1500–11.
31. Chen Q, Jin T, Qi W, Mo X, Xi L. Label-free photoacoustic imaging of the cardio-cerebrovascular development in the embryonic zebrafish. *Biomed Opt Express BOE.* 2017;8:2359–67.
32. Rebling J, Estrada H, Gottschalk S, Sela G, Zwack M, Wissmeyer G, et al. Dual-wavelength hybrid optoacoustic-ultrasound biomedicine for functional imaging of large-scale cerebral vascular networks. *J Biophotonics.* 2018;11:e201800057.
33. Ahn J, Baik JW, Kim D, Choi K, Lee S, Park S-M, et al. *In vivo* photoacoustic monitoring of vasoconstriction induced by acute hyperglycemia. *Photoacoustics.* 2023;30:100485.
34. Hsu H-C, Wang L, Wang LV. In vivo photoacoustic microscopy of human cuticle microvasculature with single-cell resolution. *J Biomed Opt.* 2016;21:56004.
35. Karlas A, Katsouli N, Fasoula N-A, Reidl M, Lees R, Zang L, et al. Multiscale optoacoustic assessment of skin microvascular reactivity in carotid artery disease. *Photoacoustics.* 2024;40:100660.
36. Karlas A, Reber J, Diot G, Bozhko D, Anastasopoulou M, Ibrahim T, et al. Flow-mediated dilatation test using optoacoustic imaging: a proof-of-concept. *Biomed Opt Express BOE.* 2017;8:3395–403.
37. Lin L, Hu P, Shi J, Appleton CM, Maslov K, Li L, et al. Single-breath-hold photoacoustic computed tomography of the breast. *Nat Commun.* 2018;9:2352.
38. Lin L, Hu P, Tong X, Na S, Cao R, Yuan X, et al. High-speed three-dimensional photoacoustic computed tomography for preclinical research and clinical translation. *Nat Commun.* 2021;12:882.
39. Na S, Russin JJ, Lin L, Yuan X, Hu P, Jann KB, et al. Massively parallel functional photoacoustic computed tomography of the human brain. *Nat Biomed Eng.* 2022;6:584–92.
40. Ivankovic I, Merčep E, Schmedt C-G, Deán-Ben XL, Razansky D. Real-time volumetric assessment of the human carotid artery: handheld multispectral optoacoustic tomography. *Radiology.* 2019;291:45–50.
41. Taruttis A, Timmermans AC, Wouters PC, Kacprowicz M, van Dam GM, Ntziachristos V. Optoacoustic imaging of human vasculature: feasibility by using a handheld probe. *Radiology.* 2016;281:256–63.
42. van den Berg PJ, Daoudi K, Steenbergen W. Review of photoacoustic flow imaging: its current state and its promises. *Photoacoustics.* 2015;3:89–99.
43. Fang H, Maslov K, Wang LV. Photoacoustic doppler flow measurement in optically scattering media. *Appl Phys Lett.* 2007;91:264103.
44. Brunner J, Beard P. Pulsed photoacoustic doppler flowmetry using time-domain cross-correlation: accuracy, resolution and scalability. *J Acoust Soc Am.* 2012;132:1780–91.
45. Fang H, Wang LV. *M*-mode photoacoustic particle flow imaging. *Opt Lett OL.* 2009;34:671–3.
46. Zhang R, Wang L, Yao J, Yeh C-H, Wang LV. *Vivo* optically encoded photoacoustic flowgraphy. *Opt Lett OL.* 2014;39:3814–7.

47. Yao J, Maslov KI, Wang LV. In vivo photoacoustic tomography of total blood flow and potential imaging of cancer angiogenesis and hypermetabolism. *Technol Cancer Res Treat*. 2012;11:301–7.
48. Wang L, Maslov K, Wang LV. Single-cell label-free photoacoustic flowoxigraphy in vivo. *Proc Natl Acad Sci*. 2013;110:5759–64.
49. Park J, Cummins TM, Harrison M, Lee J, Zhou Q, Lien C-L, et al. High frequency photoacoustic imaging for in vivo visualizing blood flow of zebrafish heart. *Opt Express OE*. 2013;21:14636–42.
50. Zhou Y, Liang J, Wang LV. Cuffing-based photoacoustic flowmetry in humans in the optical diffusive regime. *J Biophotonics*. 2016;9:208–12.
51. Zhang Y, Olick-Gibson J, Khadria A, Wang LV. Photoacoustic vector tomography for deep haemodynamic imaging. *Nat Biomed Eng*. 2024;8:701–11.
52. Galanzha EI, Sarimollaoglu M, Nedosekin DA, Keyrouz SG, Mehta JL, Zharov VP. In vivo flow cytometry of Circulating clots using negative photothermal and photoacoustic contrasts. *Cytometry A*. 2011;79:814–24.
53. Das D, Sivasubramanian K, Rajendran P, Pramanik M. Label-free high frame rate imaging of Circulating blood clots using a dual modal ultrasound and photoacoustic system. *J Biophotonics*. 2021;14:e202000371.
54. Karlas A, Masthoff M, Kallmayer M, Helfen A, Bariotakis M, Fasoula NA, et al. Multispectral optoacoustic tomography of peripheral arterial disease based on muscle hemoglobin gradients—a pilot clinical study. *Ann Transl Med*. 2021;9:36.
55. Yang J, Zhang G, Shang Q, Wu M, Huang L, Jiang H. Detecting hemodynamic changes in the foot vessels of diabetic patients by photoacoustic tomography. *J Biophotonics*. 2020;13:e202000011.
56. Ganzleben I, Klett D, Hartz W, Götzfried L, Vitali F, Neurath MF, et al. Multispectral optoacoustic tomography for the non-invasive identification of patients with severe anemia in vivo. *Photoacoustics*. 2022;28:100414.
57. Zhang Y, Hu P, Li L, Cao R, Khadria A, Maslov K, et al. Ultrafast longitudinal imaging of haemodynamics via single-shot volumetric photoacoustic tomography with a single-element detector. *Nat Biomed Eng*. 2024;8:712–25.
58. Deán-Ben XL, Ford SJ, Razansky D. High-frame rate four dimensional optoacoustic tomography enables visualization of cardiovascular dynamics and mouse heart perfusion. *Sci Rep*. 2015;5:10133.
59. Özsoy Ç, Özbek A, Reiss M, Deán-Ben XL, Razansky D. Ultrafast four-dimensional imaging of cardiac mechanical wave propagation with sparse optoacoustic sensing. *Proc Natl Acad Sci*. 2021;118:e21103979118.
60. Hatami M, Özbek A, Deán-Ben XL, Gutierrez J, Schill A, Razansky D, et al. Noninvasive tracking of embryonic cardiac dynamics and development with volumetric optoacoustic spectroscopy. *Adv Sci*. 2024;11:2400089.
61. Li L, Zhu L, Ma C, Lin L, Yao J, Wang L, et al. Single-impulse panoramic photoacoustic computed tomography of small-animal whole-body dynamics at high spatiotemporal resolution. *Nat Biomed Eng*. 2017;1:1–11.
62. Lin L, Tong X, Cavallero S, Zhang Y, Na S, Cao R, et al. Non-invasive photoacoustic computed tomography of rat heart anatomy and function. *Light Sci Appl*. 2023;12:12.
63. Lv J, Peng Y, Li S, Guo Z, Zhao Q, Zhang X, et al. Hemispherical photoacoustic imaging of myocardial infarction: in vivo detection and monitoring. *Eur Radiol*. 2018;28:2176–83.
64. Ma K, Wu S, Huang S, Xie W, Zhang M, Chen Y, et al. Myocardial infarct border demarcation by dual-wavelength photoacoustic spectral analysis. *Photoacoustics*. 2022;26:100344.
65. Zhang Y, Chen X, Liu L, Tian J, Hao L, Ran H. Photoacoustic imaging of myocardial infarction region using non-invasive fibrin-targeted nanoparticles in a rat myocardial ischemia-reperfusion model. *Int J Nanomed*. 2021;16:1331–44.
66. Zhao P, Li B, Li Y, Chen L, Wang H, Ye L. DNA-Templated ultrasmall bismuth sulfide nanoparticles for photoacoustic imaging of myocardial infarction. *J Colloid Interface Sci*. 2022;615:475–84.
67. Li F, Chen L, Zhong S, Chen J, Cao Y, Yu H, et al. Collagen-targeting self-assembled nanoprobe for multimodal molecular imaging and quantification of myocardial fibrosis in a rat model of myocardial infarction. *ACS Nano*. 2024;18:4886–902.
68. Ivankovic I, Déan-Ben XL, Haas H, Kimm MA, Wildgruber M, Razansky D. Volumetric optoacoustic tomography differentiates myocardial remodelling. *Mol Imaging Biol*. 2020;22:1235–43.
69. Lin H-CA, Déan-Ben XL, Ivankovic I, Kimm MA, Kosanke K, Haas H, et al. Characterization of cardiac dynamics in an acute myocardial infarction model by four-dimensional optoacoustic and magnetic resonance imaging. *Theranostics*. 2017;7:4470–9.
70. Taruttis A, Wildgruber M, Kosanke K, Beziere N, Licha K, Haag R, et al. Multispectral optoacoustic tomography of myocardial infarction. *Photoacoustics*. 2012;1:3–8.
71. Rahko PS. Evaluation of the skin-to-heart distance in the standing adult by two-dimensional echocardiography. *J Am Soc Echocardiogr*. 2008;21:761–4.
72. Walther A, Rippe L, Wang LV, Andersson-Engels S, Kröll S. Analysis of the potential for non-invasive imaging of oxygenation at heart depth, using ultrasound optical tomography (UOT) or photo-acoustic tomography (PAT). *Biomed Opt Express BOE*. 2017;8:4523–36.
73. Li M, Tang Y, Yao J. Photoacoustic tomography of blood oxygenation: a mini review. *Photoacoustics*. 2018;10:65–73.
74. Merčep E, Deán-Ben XL, Razansky D. Imaging of blood flow and oxygen state with a multi-segment optoacoustic ultrasound array. *Photoacoustics*. 2018;10:48–53.
75. Karlas A, Kallmayer M, Fasoula N-A, Liapis E, Bariotakis M, Krönke M, et al. Multispectral optoacoustic tomography of muscle perfusion and oxygenation under arterial and venous occlusion: a human pilot study. *J Biophotonics*. 2020;13:e201960169.
76. Masthoff M, Helfen A, Claussen J, Karlas A, Markwardt NA, Ntziachristos V, et al. Use of multispectral optoacoustic tomography to diagnose vascular malformations. *JAMA Dermatol*. 2018;154:1457–62.
77. Günther JS, Knieling F, Träger AP, Lang W, Meyer A, Regensburger AP, et al. Targeting muscular hemoglobin content for classification of peripheral arterial disease by noninvasive multispectral optoacoustic tomography. *JACC Cardiovasc Imaging*. 2023;16:719–21.
78. Soppert J, Lehrke M, Marx N, Jankowski J, Noels H. Lipoproteins and lipids in cardiovascular disease: from mechanistic insights to therapeutic targeting. *Adv Drug Deliv Rev*. 2020;159:4–33.
79. Jansen K, van Soest G, van der Steen AFW. Intravascular photoacoustic imaging: a new tool for vulnerable plaque identification. *Ultrasound Med Biol*. 2014;40:1037–48.
80. Iskander-Rizk S, van der Steen AFW, van Soest G. Photoacoustic imaging for guidance of interventions in cardiovascular medicine. *Phys Med Biol*. 2019;64:16TR01.
81. Jansen K, Steen AFW, van van der, Beusekom HMM, Oosterhuis JW, van Soest G. Intravascular photoacoustic imaging of human coronary atherosclerosis. *Opt Lett OL*. 2011;36:597–9.
82. Jansen K, Wu M, van der Steen AFW, van Soest G. Photoacoustic imaging of human coronary atherosclerosis in two spectral bands. *Photoacoustics*. 2014;2:12–20.
83. Hui J, Cao Y, Zhang Y, Kole A, Wang P, Yu G, et al. Real-time intravascular photoacoustic-ultrasound imaging of lipid-laden plaque in human coronary artery at 16 frames per second. *Sci Rep*. 2017;7:1417.
84. Wang B, Karpouk A, Yeager D, Amirian J, Litovsky S, Smalling R, et al. In vivo intravascular ultrasound-guided photoacoustic

- imaging of lipid in plaques using an animal model of atherosclerosis. *Ultrasound Med Biol.* 2012;38:2098–103.
85. Zhang J, Yang S, Ji X, Zhou Q, Xing D. Characterization of lipid-rich aortic plaques by intravascular photoacoustic tomography: ex vivo and in vivo validation in a rabbit atherosclerosis model with histologic correlation. *J Am Coll Cardiol.* 2014;64:385–90.
  86. Iskander-Rizk S, Wu M, Springeling G, Beusekom H van, Mastik F, Hekker M te L, et al. In vivo intravascular photoacoustic imaging of plaque lipid in coronary atherosclerosis. *EuroIntervention.* 2015;10:115–20.
  87. Karlas A, Kallmayer M, Bariotakis M, Fasoula N-A, Liapis E, Hyafil F, et al. Multispectral optoacoustic tomography of lipid and hemoglobin contrast in human carotid atherosclerosis. *Photoacoustics.* 2021;23:100283.
  88. Arabul MU, Heres M, Rutten MCM, van Sambeek MR, van de Vosse FN, Lopata RGP. Toward the detection of intraplaque hemorrhage in carotid artery lesions using photoacoustic imaging. *JBO.* 2016;22:041010.
  89. Muller J-W, van Hees R, van Sambeek M, Boutouyrie P, Rutten M, Brands P, et al. Towards in vivo photoacoustic imaging of vulnerable plaques in the carotid artery. *Biomed Opt Express BOE.* 2021;12:4207–18.
  90. Rekhter MD. Collagen synthesis in atherosclerosis: too much and not enough. *Cardiovascular Res.* 1999;41:376–84.
  91. Leng J, Zhang J, Li C, Shu C, Wang B, Lin R, et al. Multi-spectral intravascular photoacoustic/ultrasound/optical coherence tomography tri-modality system with a fully-integrated 0.9-mm full field-of-view catheter for plaque vulnerability imaging. *Biomed Opt Express BOE.* 2021;12:1934–46.
  92. Pleitez MA, Lieblein T, Bauer A, Hertzberg O, von Lilienfeld-Toal H, Mantele W. In vivo noninvasive monitoring of glucose concentration in human epidermis by mid-infrared pulsed photoacoustic spectroscopy. *Anal Chem.* 2013;85:1013–20.
  93. Neuschmelting V, Harmsen S, Beziere N, Lockau H, Hsu H-T, Huang R, et al. Dual-modality surface-enhanced resonance Raman scattering and multispectral optoacoustic tomography nanoparticle approach for brain tumor delineation. *Small.* 2018;14:e1800740.
  94. Karpouk AB, Wang B, Amirian J, Smalling RW, Emelianov SY. Feasibility of in vivo intravascular photoacoustic imaging using integrated ultrasound and photoacoustic imaging catheter. *J Biomed Opt.* 2012;17:96008–96001.
  95. Ren W, Deán-Ben XL, Skachokova Z, Augath M-A, Ni R, Chen Z, et al. Monitoring mouse brain perfusion with hybrid magnetic resonance optoacoustic tomography. *Biomed Opt Express BOE.* 2023;14:1192–204.
  96. Jin H, Zheng Z, Cui Z, Jiang Y, Chen G, Li W, et al. A flexible optoacoustic blood ‘stethoscope’ for noninvasive multiparametric cardiovascular monitoring. *Nat Commun.* 2023;14:4692.
  97. Gao X, Chen X, Hu H, Wang X, Yue W, Mu J, et al. A photoacoustic patch for three-dimensional imaging of hemoglobin and core temperature. *Nat Commun.* 2022;13:7757.
  98. Pang W, Yuan C, Zhong T, Huang X, Pan Y, Qu J et al. Diagnostic and therapeutic optical imaging in cardiovascular diseases. *iScience.* 2024;27.
  99. Neuschler EL, Lavin PT, Tucker FL, Barke LD, Bertrand ML, Böhm-Vélez M, et al. Downgrading and upgrading Gray-Scale ultrasound BI-RADS categories of benign and malignant masses with optoacousticTICS: A PIlot study. *Am J Roentgenol.* 2018;211:689–700.

**Publisher's Note** Springer Nature remains neutral with regard to jurisdictional claims in published maps and institutional affiliations.

Springer Nature or its licensor (e.g. a society or other partner) holds exclusive rights to this article under a publishing agreement with the author(s) or other rightsholder(s); author self-archiving of the accepted manuscript version of this article is solely governed by the terms of such publishing agreement and applicable law.